# Solidification under Forced-Flow Conditions in a Shallow Cavity

A.N. TURCHIN, D.G. ESKIN, and L. KATGERMAN

The solidification of an Al-4.5 pct Cu alloy in a shallow cavity under conditions of forced flow was studied both by fluid-dynamics simulations with solidification included and by experiments. The variation in bulk-flow velocity and initial superheat dramatically changes the macro- and microstructure, promoting grain refinement, an equiaxed-to-columnar transition (ECT), the formation of peculiar grain and dendrite morphologies, *etc*. The solidification parameters during solidification in the shallow cavity under forced-flow conditions have been determined by computer simulations and partially compared with the experimental results. The interaction between flow vortices and the progressing solidification front and its effect on structure evolution have been analyzed. Finally, quantitative correlations between microstructure, solidification, and flow parameters have been established.

DOI: 10.1007/s11661-007-9183-9


## I. INTRODUCTION

OVER the past 50 years, many attempts have been made to design special techniques with the purpose of improving and controlling the final solidified structure by forced flow. When one considers any particular casting system, one can see that the flow is present from the early stages of the process. During the casting, flow generally occurs in the bulk liquid and in the semi-solid regions. Some of the techniques have been successfully used in academic research with the aim of studying the fundamentals of solidification under forced-flow conditions: gravity flow-through systems,[1] mechanical stirring,[2] centrifugal casting,[3] application of a magnetic or electromagnetic field creating the Lorenz force,[4,5] *etc*. As experimental research has developed over the last 50 years, computational modeling and simulation have been widely used in the last two decades as cost-saving tools for the prediction and interpretation of the results. Using these two approaches in combination leads to a deeper understanding of the effects of melt flow as a result of natural and forced convection on the solidification phenomenon in metallic alloys, *i.e*., (1) the morphology of grains and their deflection toward incoming flow,[1–5] (2) the columnar-to-equiaxed transition and grain morphology,[4] and (3) the change of segregation pattern.[4,5,6]

Forced flow applied to the bulk of the molten metal interacts with the growing solid producing the distortion of the solid-liquid interface,[1] altering the shape of the mushy zone[7] and affecting the solidification parameters.[8] Depending on the nature of the flow and the initial velocity, oscillation (vortices) of various magnitudes may occur at the solidification front.

A.N. TURCHIN, Ph.D. Student, D.G. ESKIN, Senior Scientist, are with the The Netherlands Institute for Metals Research, 2628CD, Delft, The Netherlands. Contact e-mail: a.turchin@nimr.nl L. KATGERMAN, Professor, is with the Department of Materials Science and Engineering, Delft University of Technology, 2628CD, Delft, The Netherlands.

Manuscript submitted December 13, 2006.

However, many questions are still far from being understood completely. How does the forced flow and, in particular, the vorticity at the solidification front affect the macrostructural features? How does the forced flow influence the microstructure evolution?

The present study is aimed at analyzing the effects of macroinstabilities at the solidification front on macro- and microstructural features. The solidification under forced-flow conditions in the chill with a shallow rectangular cavity is proposed to create the vortex structure at the solid-liquid interface while solidification progresses. The combined approach based on fluid dynamics calculations and experimental work is implemented to determine quantitatively the solidification parameters, *i.e*., the local solidification time, rate, and thermal gradient, depending on the flow and heat regimes. In addition, the correlations between the structural parameters, the associated shape of the mushy zone, and the forced flow have been established.

## II. EXPERIMENTAL PROCEDURE

The objectives of the present study were as follows: (1) to obtain the solidification parameters during solidification in a shallow cavity under forced-flow conditions, (2) to examine the interaction of vortices with the progressing solidification front and their effect on structure evolution, and (3) to determine the quantitative correlations between microstructure and forced-flow parameters.

To accomplish the intended goals, a controllable system that provides a constant unidirectional bulk flow along the solidification front has to be selected. The rotating chill, centrifugal or electromagnetic castings, *etc*. can provide the bulk flow along the solidification interface. However, a closed system such as this would cause some inconveniences associated with difficult flow velocity control, complicated flow pattern, and high velocities. Therefore, an already complex solidification

process becomes even more unclear. The experimental setup finally chosen produces a constant unidirectional bulk flow and provides sufficient control of the bulk-flow velocity.[9] The setup consists of an electromagnetic pump and a specially designed flow-through system with a built-in, water-cooled cooper chill; this system is described in detail elsewhere.[9] The solidification under static casting with either water-cooled or preheated chill, and under different forced-flow conditions occurs on the chill with the rectangular cavity 100 × 10 mm.

A model Al-Cu alloy with 4.5 pct copper was prepared using 99.95 pct pure aluminium and an Al-47.7 pct Cu master alloy (here and elsewhere in this article, weight percents are used). The first reason the Al-Cu system was chosen was because of a relatively low melting temperature and a simple eutectic-type phase diagram in the Al-rich corner of the system. The alloys in this corner have a wide solidification range and high thermal conductivity, both of which promote a large two-phase region. The second reason the Al-Cu system was chosen was because the physical properties and solidification behavior of Al-Cu alloys are well known and understood; these can be used for computer simulations and additional modeling.

During the experiments, the temperature is measured at several points: in the liquid bath, at the entrance to the launder, at the different distances above the chill surface, and at the chill-melt interface. The data are recorded by a computer equipped with a National Instruments* data acquisition card and software.

*National Instruments is a trademark of NI, Austin, TX, USA.

K-thermocouples (0.2-mm wires) were placed at the different distances from the chill surface in the solidified melt (1, 5, and 10 mm) and in the chill.

In order to accurately control the most important process parameter, the linear melt-flow velocity, a video recording of the flowing melt together with the measurements of the outflow weight was made. The measurement results show that a condition of steady flow velocity is achieved during the experiments. The experiments were performed at melt-flow rates ranging from 0.03 to 0.30 m/s and at melt temperatures of 973 and 993 K. The melt temperatures correspond to a melt superheat of 55 and 75 K, respectively.

After the experiments, samples were sliced in the middle section along the longitudinal axis of the symmetry, and were polished and etched for examination of the macro- and microstructure in an optical microscope Neophot 30**. In order to reveal the macrostructure of the whole section, the samples were polished and etched with 45 mL HCl, 15 mL $HNO_3$, 15 mL HF, and 25 mL $H_2O$ solution (Tucker's reagent). The samples were electro-oxidized at 20 VDC in a 3 pct $HBF_4$ water solution, to reveal the grain structure under polarized light. One of the aims of the present work is to correlate the microstructure, solidification, and flow parameters. Structure parameters (Figure 1) such as primary ($\lambda_1$) and secondary dendrite arm spacing ($\lambda_2$) were measured semi-automatically, using the measurement software AnalySIS† (Ver.5.0) on photographs taken from areas of interest.

**Neophot 30 is a product of Carl Zeiss, Jena, Germany.

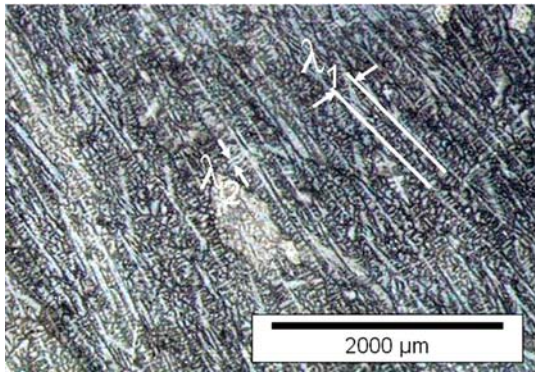


Fig. 1—Definition of primary ($\lambda_1$) and secondary ($\lambda_2$) dendrite arm spacing in an Al-4.5 pct Cu alloy; flow direction is from left to right.

†AnalySIS is a trademark of Olympus Soft Imaging Systems, Munster, Germany.

## III. GENERAL COMPUTATIONAL PROCEDURE

Computer simulations of solidification under forced-flow conditions of an Al-4.5 pct Cu alloy were performed with the commercial software Flow-3D‡ (Ver. 9.1). The code solves the Navier–Stokes equations for fluid flow, using a finite-volume approach. A hybrid model proposed by Oldenburg and Spera[10] for solidification and convection that considers the dependence of viscosity on solid fraction in the slurry region and the dependence of permeability on solid fraction in the mushy zone is incorporated in Flow-3D. Equations are solved iteratively using the minimum time-step of $10^{-9}$ s. The two-dimensional domain 140-mm long and 40-mm high was divided into 35,000 cells. A coupled computation of flow and thermal fields is applied using a uniform structured mesh. The flow with free surface and an identical laminar Blasius boundary-layer thickness of 0.005 m was studied at different inlet flow velocities. Previously, the code was validated against experimental results, including the following: (1) mold filling,[11] (2) solidification,[11,12] and (3) flow pattern.[13]

‡Flow-3D is a trademark of Flow Dynamics Inc., Santa Fe, NM.

In the simulations, the melt is flowing from the left to the right of the computational domain at a constant velocity and melt temperature. Solidification starts as

Table I. Inlet Velocity ($V_X$), Inlet Temperature ($T_{inlet}$), Cooling Conditions, and Experimental Conditions in Computer Simulations and Experiments

| $N_0$ | $V_x$, m/s | $T_{inlet}$, K | Chill | Experiment |
|---|---|---|---|---|
| 1 | — | 973 | cooled | no-flow |
| 2 | — | 973 | preheated | no-flow |
| 3 | 0.05 | 973 | cooled | forced flow |
| 4 | 0.15 | 973 | cooled | forced flow |
| 5 | 0.30 | 973 | cooled | forced flow |
| 6 | 0.02 | 993 | cooled | forced flow |
| 7 | 0.12 | 993 | cooled | forced flow |
| 8 | 0.16 | 993 | cooled | forced flow |

the flowing melt is brought into contact with the chill surface, and proceeds under conditions of constant melt flow along the solidification front. A series of calculations is performed in order to obtain the solidification behavior under forced-flow conditions and compare it to flow patterns in the cavity without solidification. The evolution of solid fraction and temperatures is calculated as a function of time and position in the sample. The chill is bound by ceramic material and all interfaces are impermeable to the liquid alloy. The interface between chill and melt flow is no-slip. The free surface of the flowing melt is deformable, since we consider the surface tension effect.

The boundary conditions applied to different sides of the computational domain are as follows. To model the cooling, the Dirichlet condition at the bottom of the computational domain taken from the experimental measurements is applied. The top of the domain is considered adiabatic. The boundary conditions at the inlet are the constant flow velocity and the melt temperature (Table I). The outlet boundary is a zero heat flux. The heat transfer at the interfaces between the ceramic material (before and after the chill) and the melt flow is determined using a constant heat transfer coefficient of 100 W/m$^2$ K; between the copper chill and the melt flow, it is 1500 W/m$^2$ K.

The thermophysical properties and phase-diagram parameters of the model alloy (Al-4.5 pct Cu) used in the present work are described elsewhere.[14]

The solidification model under forced-flow conditions was validated against experimental temperature measurements obtained in various locations in the flowing melt and in the chill. The comparison of experimental and numerical data demonstrated a reasonable agreement, as shown in Section IV. Finally, the solidification parameters correlated further with structure parameters were determined from calculated and measured temperature distributions.

In addition, to simulate the settling of fragments in the beginning of the solidification process, the particles-transport calculation in the flowing melt without solidification has been performed for an inlet bulk velocity of 0.15 m/s. The fragments were modeled as spherical particles with the size 50 $\mu$m and the density 2750 kg/m$^3$. The particles were generated at the upstream part above the chill surface in the melt flow, with a generation rate of 10 s$^{-1}$.

## IV. RESULTS

### A. *Solidification and Thermal History: Comparison with Experimental Results and Estimation of Solidification Parameters*

In order to attain the solidification parameters of an Al-4.5 pct Cu alloy solidified under various flow velocity and melt temperature conditions, the experimentally measured and calculated cooling curves have been compared. As an example, the cooling curves obtained in the central part and at different distances from the chill surface during solidification in the cavity for the "no-flow" conditions with the cooled chill, and for inlet velocities of 0.05 and 0.15 m/s are shown in Figure 2. It can be seen that the temperature distribution differs depending on the flow conditions. The temperature evolution for the sample obtained under the no-flow condition exhibits a typical time-dependent cooling curve (Figure 2(a)) with rapidly decreasing temperature. Under forced flow, the effective cooling rate decreases (Figures 2(b) and (c)). The comparison of the calculated and measured temperatures on the same graph shows an adequate agreement with the temperature difference of 3 to 4 pct (10 to 15 K) that allows one to consider the calculated thermal field along the chill to be correct within the obtained margin of error.

The temperature gradient profile along the chill cavity shows the tendency to decrease in the direction of flow (Figure 3). Interestingly enough, the central region of the cavity is characterized by the identical thermal gradient for different flow conditions (4 to 4.5 K/mm). This fact provides us the opportunity to compare the samples obtained under the same thermal gradient and different flow regimes when considering the same dendrite morphology (columnar).

Finally, the calculated cooling curves and the experimental measurements have been also used to generate other solidification parameters, such as the solidification rate and cooling rate, which are summarized for the all experimental samples obtained at the melt superheats 55 and 75 K in Tables II and III, respectively.

### B. *Cavity-Driven Flow Problem*

For a better understanding of the interaction between forced flow and solidification in the present experimental scheme, it is desirable first to reveal the flow pattern

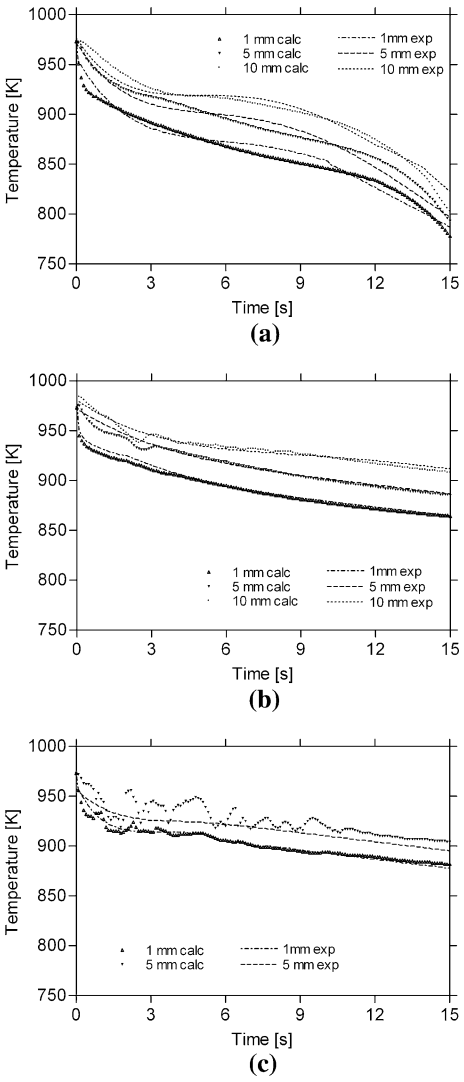


Fig. 2—Comparison of measured and calculated temperature curves taken in the melt and upon solidification at 1, 5, and 10 mm from the chill surface for the samples (*a*) without forced flow and obtained at flow velocities of (*b*) 0.05 m/s and (*c*) 0.15 m/s.

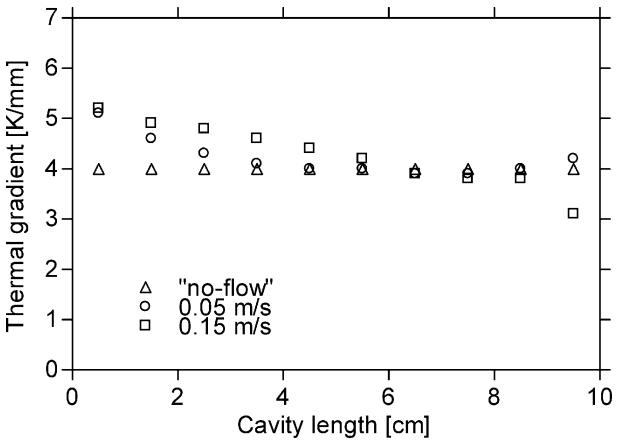


Fig. 3—Calculated thermal gradient averaged over the height between 1 and 10 mm along the chill cavity for the no-flow condition with cooled chill and for flow velocities of 0.05 and 0.15 m/s.

in a cavity without heat transfer. Figure 4 shows the result of such calculations. The flow can be characterized as follows: constant forced flow above the cavity interacts with the flow in the cavity, resulting in the formation of a vortex structure in the cavity due to a high velocity gradient in the shear layer.

The cavity flow fields were studied at two inlet velocities, 0.05 and 0.15 m/s (Figure 4). As can be seen, after a short time, the flow detaches itself from the upstream edge of the cavity due to the velocity gradient in the shear layer, which results in the development of the primary vortex (Figure 4(a) after 0.4 seconds). As time progresses, several vortices can be observed in the cavity below the shear layer, traveling in the same direction as the initial flow. By the time the vortex reaches the downstream corner of the cavity, it merges in the mainstream forced flow. The flow pattern indicates the Kelvin–Helmholz instabilities (K-H instabilities) in the shear layer.[15]

When the inlet velocity increases, the flow in the cavity becomes more chaotic (Figure 4(b)). The significant feature of this flow is the strong interaction between the large clockwise-rotating vortex with the constantly incoming forced flow promoting a less structured vorticity in the cavity, as compared to the smaller velocity. It is worth noting that the shear layer clearly visible in Figure 4(a) vanishes when the flow velocity increases.

### C. *Cavity-Driven Flow Problem with Solidification*

Let us now consider the flow pattern in the presence of solidification under forced-flow conditions. The instantaneous velocity vectors at different times and the corresponding solid-fraction contours indicate the interaction between the forced flow and the growing solid (Figure 5). The vortex structure in the cavity is similar to the vorticity observed without heat transfer. When comparing Figure 5 with the results described in Section IV–B at the same flow velocity of 0.05 m/s, several observations can be made. Specifically, weaker K-H instabilities are observed in the shear layer when solidification is included. Due to the dynamic decrease of the cavity geometric $D/L$ ratio ($L$ = length, and $D$ = depth of the cavity), the vortex structure is affected. As time progresses, the vortices become elongated. After 4 seconds, the longitudinal vortex is found at the growing solidification front and K-H instabilities are hardly noticed (Figure 5(a)). As can be seen from Figure 5(b), the flow structure at the higher flow velocity looks similar to the flow pattern obtained without heat transfer (Figure 4(b)). However, there are considerable differences in the size of the vortices as a result of progressing solidification and, consequently, the $D/L$ cavity ratio changes. Interestingly enough, Figure 5(b) demonstrates the development of counter-clockwise vortices in the flow structure. Additionally, while the free surface for the velocity of 0.05 m/s remains almost undisturbed, the waves can be observed when the velocity increases.

In summary, the high-velocity gradient between the forced flow and the flow in the cavity results in the

**Table II. Solidification Parameters for the No-Flow Condition and for Different Flow Velocities at the Same Initial Superheat 55 K, as Obtained from Computer Simulations and Experimental Measurements ($\dot{T}$ = Cooling Rate, $G$ = Thermal Gradient, and $V$ = Solidification Rate)**

| Conditions | $\dot{T}$, K/s | $G$, K/mm | $V$, mm/s | $G/V$ |
|---|---|---|---|---|
| no-flow cooled chill | 7.6 to 10.6 | 4 to 4.3 | 1.7 to 2.65 | 1.5 to 2.5 |
| no-flow preheated chill | 0.3 to 6.2 | 4 to 6.1 | 0.075 to 1.55 | 2.6 to 81.3 |
| 0.05 m/s | 0.35 to 2.3 | 3.9 to 6.7 | 0.05 to 0.58 | 6.7 to 134 |
| 0.15 m/s | 0.28 to 1.3 | 3.1 to 5.2 | 0.05 to 0.25 | 12.4 to 104 |
| 0.30 m/s | 0.18 to 1.4 | 2.6 to 6.1 | 0.025 to 0.22 | 11.8 to 244 |

**Table III. Solidification Parameters for Different Flow Velocities $V_x$ and at the Same Initial Superheat 75 K, as Obtained from Computer Simulations and Experimental Measurements ($\dot{T}$ = Cooling Rate, $G$ = Thermal Gradient, and $V$ = Solidification Rate)**

| $V_x$, m/s | $\dot{T}$, K/s | $G$, K/mm | $V$, mm/s | $G/V$ |
|---|---|---|---|---|
| 0.02 | 0.8 to 11.7 | 9 to 15 | 0.06 to 1.3 | 7 to 216.6 |
| 0.12 | 0.3 to 2.7 | 9 to 17 | 0.02 to 0.31 | 29 to 850 |
| 0.16 | 0.3 to 1.44 | 9 to 18 | 0.02 to 0.16 | 56 to 900 |

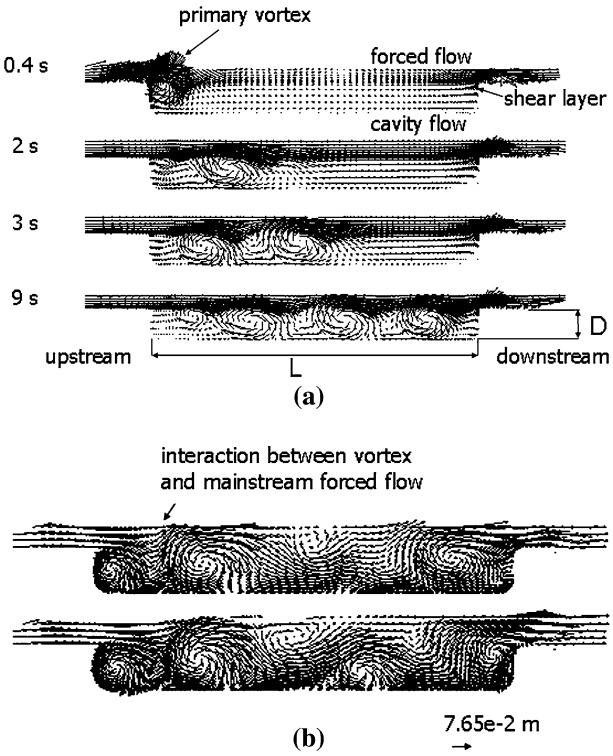


Fig. 4—Velocity vector plots at different times after initiation of flow for the inlet velocities (*a*) 0.05 and (*b*) 0.15 m/s; $L$ = length, and $D$ = depth of the cavity.

development of K-H instabilities that tend to stretch in a longitudinal direction when the geometric ratio of the cavity decreases due to progressing solidification.

### D. *Structure Development*

#### 1. *General observations*

An Al-4.5 pct Cu alloy was initially solidified under no-flow conditions, as the melt was poured either into water-cooled or preheated cavity chill. The resulting longitudinal macrostructures of the samples consist of equiaxed and columnar grains. In the latter case, the columnar grains are slightly inclined from the normal to the chill surface as a result of the pouring momentum.

Figure 6 shows two typical macrostructures of the longitudinal section of an Al-4.5 pct Cu alloy obtained during solidification in the cavity under conditions of constant forced flow along the solidification front. Depending on the flow conditions, the macrostructure of samples consists either entirely of columnar grains deflected toward the incoming flow (Figure 6(a)) or of a zone of equiaxed grains with a columnar zone on top in the central part of the sample, expanding in the direction of the downstream edge with respect to the bulk-flow direction. Equiaxed-to-columnar transition (ECT) is clearly seen at the bottom of the sample (Figure 6(b)).

The longitudinal macrostructure of the samples obtained under forced-flow conditions can be conditionally divided into three zones. Zone A is the region close to the upstream edge, with regard to the initial flow, while zone C is the region of the downstream edge of the cavity. Therefore, zone B is the central part of the cavity.

During the experiment, zone A is constantly affected by the hottest melt flow and the highest thermal gradient. However, due to heat extraction from the bottom and side wall, the solidification onset occurs after the first seconds of the experiment. The same heat extraction conditions are typical for zone C. However, the melt temperature and the flow pattern are different. According to the computational results, the boundary between zones A and B is about the reattachment length of the forced flow and the position of the clockwise vortex (Figure 5(b)). Zone B is the zone most affected by vortices traveling counter-clockwise or clockwise (Figure 5).

It is also possible to separate some zones in the vertical section (Figure 7). It is found that the zone close to the chill surface (zone 1) may exhibit different structures, such as (1) a coarse dendritic equiaxed structure, (2) a globular equiaxed structure, and (3) an

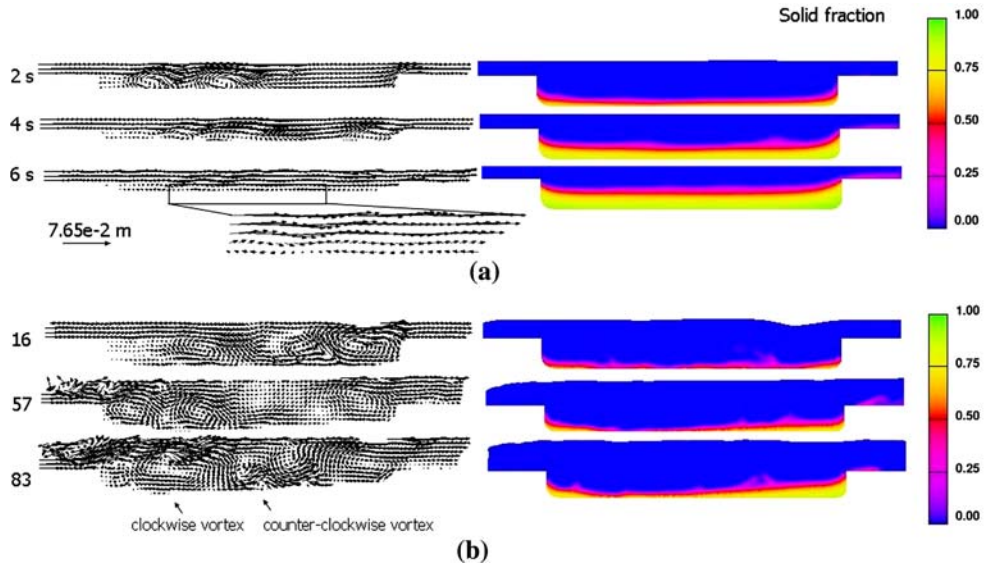


Fig. 5—Velocity vector plots and solid-fraction contours at different times for inlet velocities of (*a*) 0.05 m/s and (*b*) 0.15 m/s; flow direction is from left to right, and the bottom is the chill surface.

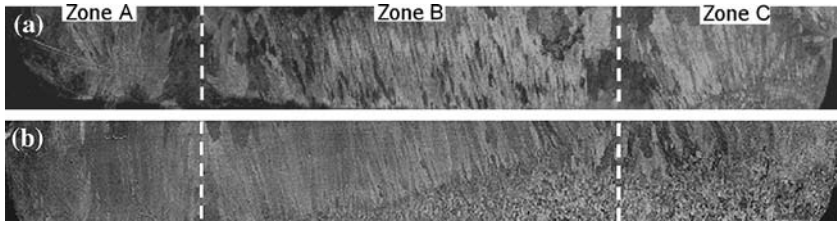


Fig. 6—Typical macrostructures of an Al-4.5 pct Cu obtained under different forced-low conditions: (*a*) 0.05 m/s, superheat 55 K; and (*b*) 0.15 m/s, superheat 55 K; length of the sample is 100 mm, and flow direction is from left to right.

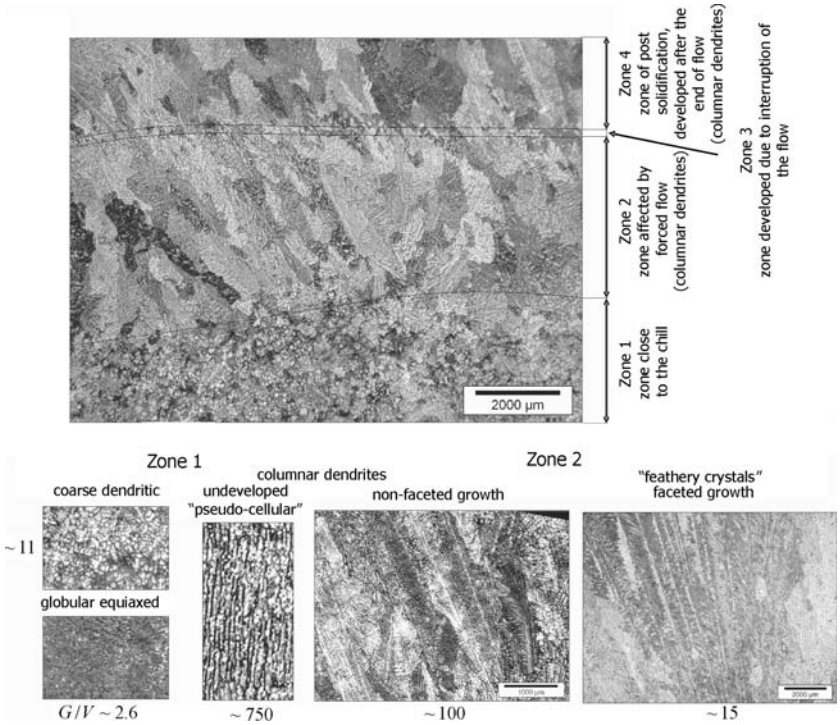


Fig. 7—Typical microstructures of an Al-4.5 pct Cu alloy obtained under different forced-flow conditions with the indicated $G/V$ ratio.

undeveloped columnar structure. The zone affected by the forced flow (zone 2) consists of columnar dendrites and in some cases of "feathery crystals" deflected toward the incoming flow. The next zone (zone 3) marks the solidification front. Finally, at the top of the sample, there is a zone (zone 4) developed after the end of the experiment that consists of columnar dendrites, but with a completely different, always finer, internal structure as compared with zone 2 (Figures 7 and 8). The dimensions of each zone may vary depending on the flow conditions.

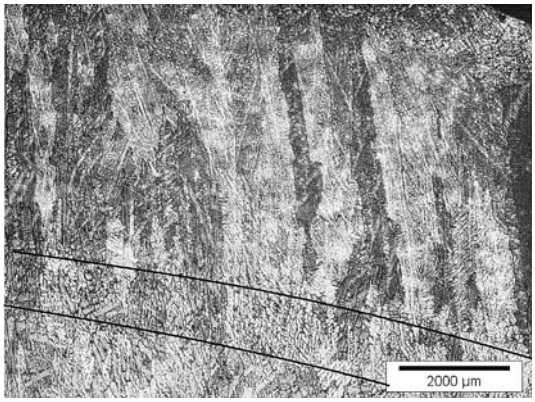


Fig. 8—Transition between zones 2 through 4.

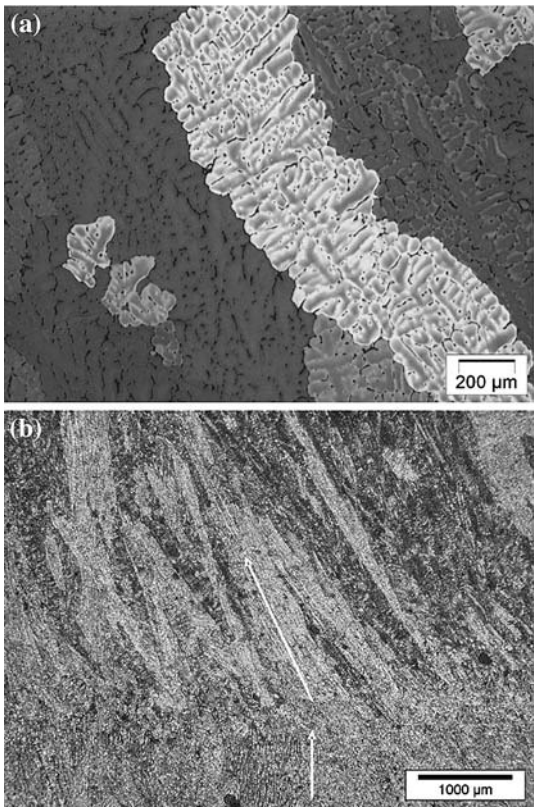


Fig. 9—(*a*) Pronounced branch growth of individual grains on the downstream side (0.05 m/s, superheat 55 K) and (*b*) change in growth direction of columnar grains shown with arrows (0.12 m/s, superheat 75 K).

As shown in the present and earlier published works, *e.g.*, References 1, 4, and 9, the grains growing in the flowing melt are deflected toward the incoming flow. However, it was often observed that (1) dendrites are deflected in a downstream direction, typically, in the area close to the upstream edge of the cavity; and (2) the growth orientation may change while the solidification proceeds. One example of growth change is shown in Figure 9(b). Figure 10 shows a correlation between the calculated isotherms and the growth orientation. It can be seen that the deflection of grain growth has a certain relation to the isotherms (Figures 6 and 10, respectively).

2. *Microstructure evolution*

In order to study the effect of forced convection on the microstructure features, the melt flow is applied perpendicular to the direction of the heat flow. Observations show that the forced flow has a significant influence on the dendrite growth, namely, the growth direction and the morphology of dendrites during solidification. Since the convection effects, particularly for Al-4.5 pct Cu, can be negligible only for a sample less than 1 mm in size,[16] it is rather impossible within the scope of the current experimental procedure to obtain a sample solidified exclusively under a diffusive regime. While the dendritic structure growing in a stagnant melt exhibits the symmetrical growth of the dendrite arms, under conditions of forced flow the growth in the upstream direction is favored due to the solute gradient in the liquid.[17]

However, in the present work, at low bulk-flow velocities, some of the columnar grains are found to have more pronounced growth of higher-order arms on the downstream side (Figure 9(a)) or to have changed the initial growth orientation (Figure 9(b)).

Peculiar morphologies have been further observed in the structure of samples solidified under forced-flow conditions with a highly superheated melt ($> 55$ K) and upon slow bulk flow ($< 0.05$ m/s). Figure 11(a) shows typical feathery crystals consisting of parallel lamellae growing into the incoming flow. The electro-anodizing of samples reveals that these lamellae are separated either by wavy or by straight boundaries. The latter is a twinned boundary. Another morphology typical for the high thermal gradient and a solidification rate less than 1 mm/s is presented in Figure 11(b). As can be seen, the dendrite arms, growing on the upstream side at 40 deg from the primary trunk, exhibit a curved, woven-type shape and are directed to the incoming flow.

Since the solidification parameters, *e.g.*, the cooling rate and the solidification rate, vary depending on the position from the chill surface, solidification under forced-flow conditions in the present scheme of experiments belongs to the unsteady-state regime, which represents most of the industrial casting processes. In order to determine the correlations between the microstructure features and the flow pattern, a "refined" method has been proposed in the present work. The solidification parameters for different heat and flow regimes are obtained with the aid of computer simulations and validated against experimental temperature

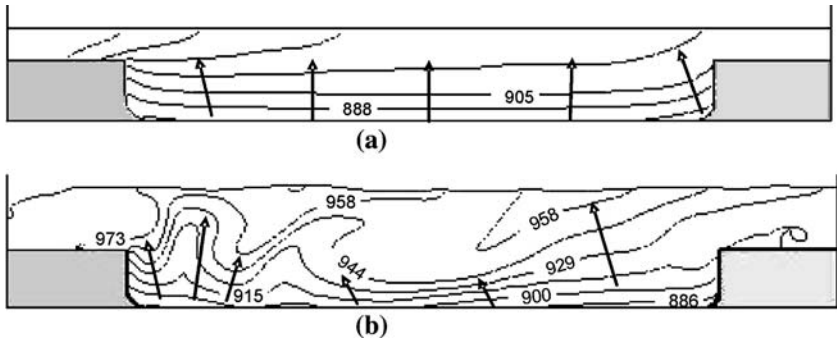


Fig. 10—Calculated isotherms with schematically shown grain growth directions (corresponds to Figure 6): (*a*) 0.05 m/s and (*b*) 0.15 m/s, superheat 55 K. Flow direction is from left to right.

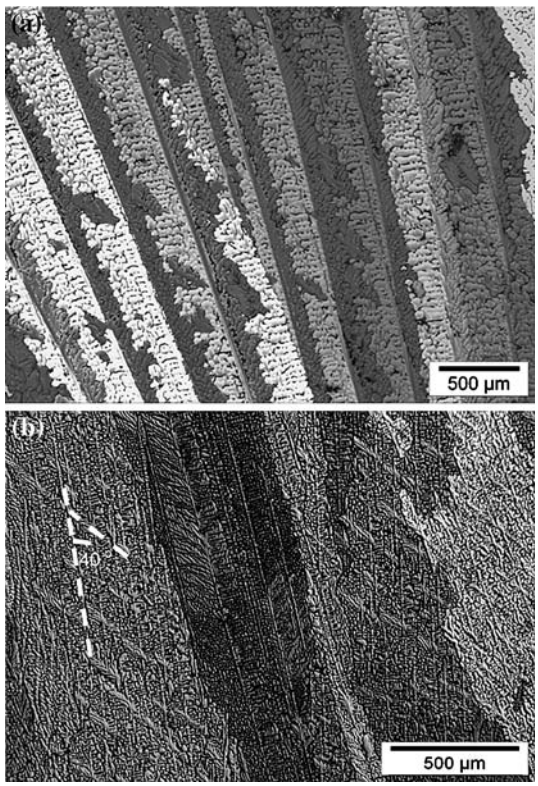


Fig. 11—Dendrite structure of an Al-4.5 pct Cu alloy obtained under forced-flow conditions at (*a*) solidification rate of 0.6 mm/s and thermal gradient of 9 K/mm and (*b*) 0.7 mm/s, 15 K/mm. Flow direction is from left to right.

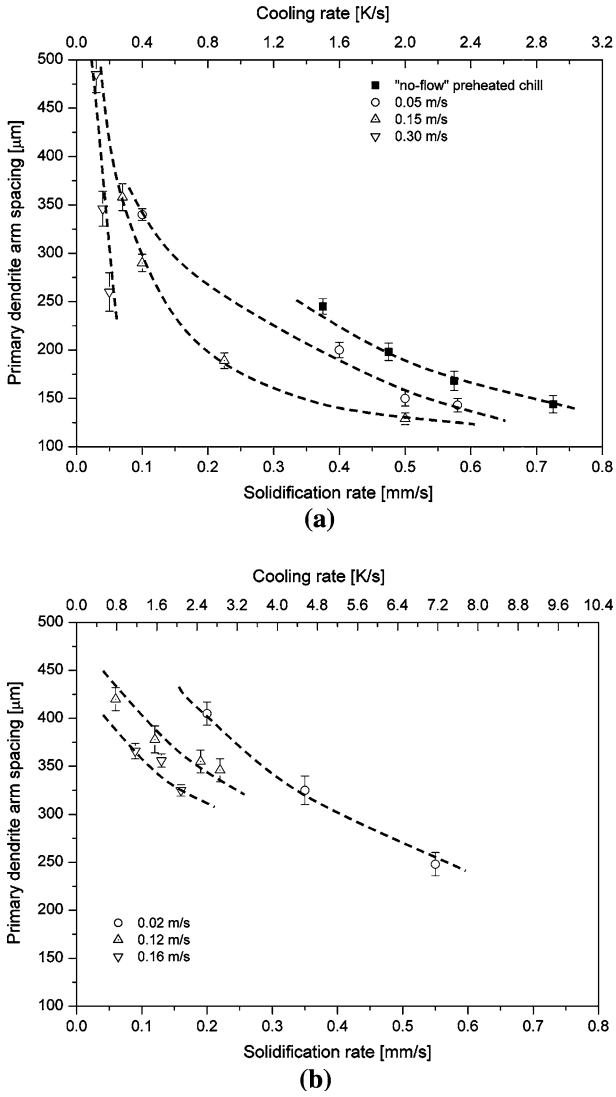


Fig. 12—Primary dendrite arm spacing ($\lambda_1$) depending on solidification rate for an Al-4.5 pct Cu alloy obtained under different flow conditions and superheat of (*a*) 55 K ($G$ = 4 to 4.5 K/mm) and (*b*) 75 K ($G$ = 13 K/mm). Trend lines are added to the plot for clarity.

measurements. As a result, it is shown that the microstructures of the samples, although developed under variable solidification conditions such as the solidification rate and time, have some common constitutive parameters, *e.g.*, the thermal gradient (Figure 3). Thus, the similarity, especially, in the thermal gradient allows one to compare the microstructure features formed at different flow regimes.

The primary dendrite arm spacing ($\lambda_1$) is plotted in Figures 12(a) and (b) as a function of the solidification rate for different flow velocities at a thermal gradient of 4 to 4.5 K/mm for superheat 55 K and at 13 K/mm for superheat 75 K, respectively (Figure 12). The accelerated flow results in a decrease in the primary dendrite arm spacing; at the same time, an increase in the solidification rate decreases the distance between

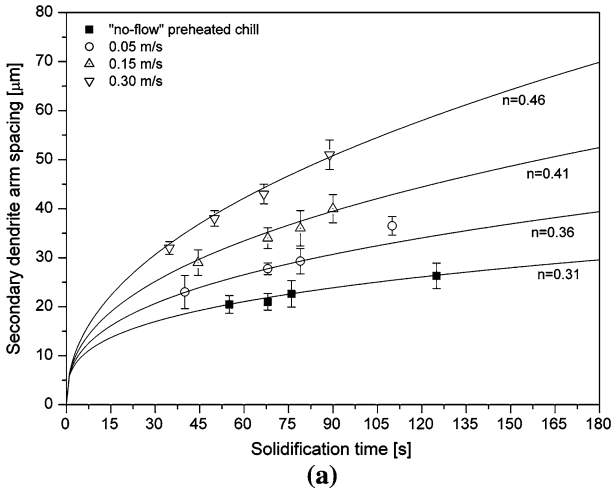


Fig. 13—Secondary dendrite arm spacing ($\lambda_2$) depending on solidification rate for an Al-4.5 pct Cu alloy obtained under different flow conditions and (*a*) superheat of 55 K ($G$ = 4 to 5 K/mm) and (*b*) 75 K (G = 13 K/mm). The measured values were fitted to Feurer[22] equation (Eq. [2]).

primary trunks. This tendency is valid for both cases with different superheats and thermal gradients.

The dependence of the secondary dendrite arm spacing ($\lambda_2$) on the solidification time, flow velocity, and superheat is shown in Figure 13. Although it has long been known that increasing solidification time coarsens the structure, the effect of the forced flow itself has rarely been considered. The present results exhibit the tendency of the microstructure to coarsen both with the increasing solidification time and the flow rate, namely, at different superheats and thermal gradients.

## V. DISCUSSION

### A. *Correlation between Thermal Field and Structure Morphology*

Flow over a cavity is prone to oscillations. Vortices in the flow are known to have a marked influence on shear-stress distribution and heat-transfer rates. The oscillations are influenced by the free-surface wave effect and by coupling the oscillations of the shear layer over the cavity with the flow inside the cavity. In particular, for incompressible flow, so-called K-H instabilities are caused by the interaction between the shear layer and the flow within the cavity.[15] Due to these instabilities, unsteady vertical structures are generated that travel along the cavity to produce fluctuations in velocity and heat distribution. With solidification progressing, the vortices tend to alter their structure from circular to longitudinal, due to the changing geometrical aspect ratio of the cavity.

The constant inflow of melt changes the solidification parameters, such as the solidification rate $V$ and the thermal gradient $G$, strongly affecting the structure morphology. In the present work, the following structure morphologies have been observed: developed dendritic columnar, undeveloped columnar, and equiaxed.

The developed dendritic columnar structure is the most common morphology in the present work. As can be seen from Tables II and III, the flow lowers the solidification rate, while the thermal gradient remains almost the same. This results in an increasing $G/V$ ratio and a corresponding morphology change from a dendritic columnar to an undeveloped columnar structure. In spite of the fact that the highest $G/V$ ratio in Tables II and III did not fall in a region of undeveloped columnar growth,[18] this type of structure has been found locally close to the chill surface, especially in experiments with high superheated melt flow (Figure 7). It means that a local shift in the thermal gradient or the solidification rate may occur due to the flow phenomenon.

The zone of equiaxed grains extending from the central part to the downstream edge of the cavity was observed at relatively high bulk-flow velocities, starting from 0.10 m/s, and at the low superheat 55 K. This ratio of velocity and superheat provides, most probably, an optimum heat inflow for the generation and survival of dendrite fragments in the present experimental scheme. The results of computer simulations show that this area is solidified at a thermal gradient ranging from 2.6 to 4.2 K/mm and at a solidification rate of 0.1 to 0.25 mm/s. This $G/V$ ratio corresponds to the transition between equiaxed and columnar morphology.[18] Thus, the nucleation along the chill wall in the form of equiaxed or columnar dendrites can occur. On the other hand, it is reasonable to assume that, due to the strong flow, these dendrites may detach from the chill. The detached grains or fragments (marked with a circle, in Figure 14) could be then transported by the forced flow from the upstream part of the cavity and, finally, settle in the downstream corner of the cavity. In summary, the following phenomena may contribute to formation of the zone of equiaxed grains: (1) the transport and continuous deposition of the detached dendrites along the chill wall by the forced flow and (2) the detachment of the slender dendrite arms and their transport to downstream edge of the cavity. The macrostructural features, such as tiny columnar dendrites, duplex (coarse and fine) internal structure, *etc.*, observed in this zone support the suggested mechanisms.

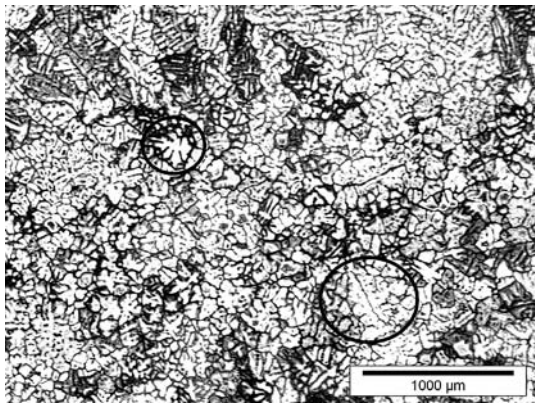


Fig. 14—Possible detached grains and fragments in the zone of equiaxed grains in the downstream corner of the cavity (marked with circle).

In order to verify the possibility of fragmentation, a model of stresses within a dendrite arm induced by the flow proposed by Pilling and Hellawel[19] has been used:

$$\sigma = \frac{6\eta l^2 \upsilon}{r^3} \quad [1]$$

where $\sigma$ is the skin stress in the dendrite arm, $\upsilon$ is the inlet velocity, $\eta$ is the melt viscosity, $r$ is the radius, and $l$ is the length of the dendrite arm. Several assumptions are made for this analysis: the linear velocity has been considered and the surroundings of a single dendrite have not been taken into account. For a bulk-flow velocity of 0.30 m/s and structural parameters of an Al-4.5 pct Cu alloy, it can be shown that the skin stress in the dendrite arm may exceed the yield stress for the Al-4.5 pct Cu alloy (Figure 15). This result brings one to the conclusion that the plastic deformation of dendrites due to the forced flow may already occur at the earlier stage of solidification (small dendrite radius and length) and at high bulk velocity, since velocities in vortices can increase several times due to accelerating flow.

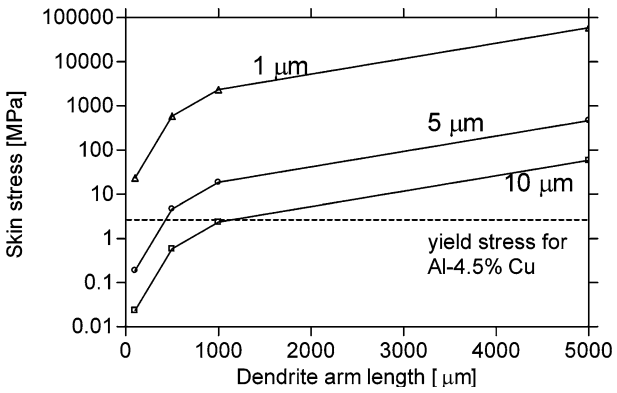


Fig. 15—Skin stress in the dendrite arm of an Al-4.5 pct Cu alloy depending on dendrite arm length and radii (indicated on the plot) for the bulk-flow velocity of 0.30 m/s; dotted line is the yield stress for an Al-4.5 pct Cu alloy close to the melting temperature, taken from Ref. 19.

The argument concerning the formation of the zone of equiaxed grains as a result of grain transport can be further supported by computer simulations of particle motion in the forced flow without heat transfer. The inlet bulk velocity is 0.15 m/s. As can be seen from Figure 16, after the first seconds, the particles are concentrated in the bottom right corner of the chill. If solidification takes place in the cavity close to downstream edge under conditions of low thermal gradient (Figure 3) in this area, plenty of fragments can be produced by the forced flow. Additionally, the survived fragments from the other places of the chill can be transported to this region and settled there.

It is also worth mentioning that the macrosegregation pattern reported earlier[21] indicates negative segregation in the region of the equiaxed dendrites. From the reasons given here, it can be argued that the "floating" fragments may contribute to the negative segregation during the casting.

This discussion seems to support the equiaxed zone formation, due to several simultaneous mechanisms, such as (1) the detachment of the growing dendrites by the forced flow, (2) the fragmentation of slender dendrite arms, and (3) their continuous deposition in the downstream corner of the cavity.

The phenomenon of ECT in the case with the cavity chill can be attributed to the termination of the fragmentation and the settling processes, with the growth of the columnar dendrites under conditions of thermal gradient. Let us discuss the experiment with the inlet velocity of 0.15 m/s in more detail (Figure 6(b)). After the onset of solidification, the fragments may form as a result of either the detachment of the equiaxed and columnar dendrites at the chill surface or the fragmentation of their slender dendrite arms. These fragments are either immediately removed from the chill zone by the constantly coming forced flow or continuously settled in the downstream edge of the chill. In the meantime, the columnar dendrites keep growing at the upstream edge due to the highest thermal gradient and, at the same time, the strong heat extraction in this region (Figures 3 and 17). While the progressing solidification facilitates fragmentation due to the branching of dendrites, on the one hand, it increases the probability the fragments will be removed from the chill zone by the melt outflow due to the decrease in the geometrical ratio of the cavity (Figure 3). At the same time, due to the gap between the family of columnar dendrites at the upstream corner and the settled fragments at the downstream corner, the preferable thermal conditions promote the free growth of columnar dendrites that are clearly distinguished on Figures 6(b) and 17.

Several dendrite morphologies were reported in Section IV as typical of certain conditions obtained under forced flow. Feathery growth was more than once discussed, *e.g.*, by Henry *et al.*,[22] and is found in the present work to be favored at the thermal gradient ~10 K/mm and the solidification rate of less than 1 mm/s (Figure 11(a)). The dendrite morphology shown in Figure 11(b) has been obtained earlier in aluminium alloys under conditions of no convection in

Fig. 16—Particle distribution in an Al-4.5 pct Cu alloy in the cavity of the chill; flow direction is from left to right.

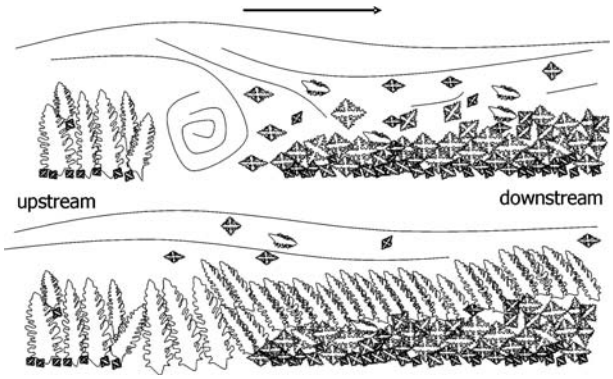


Fig. 17—Schematic illustration of progressing solidification under forced-flow conditions; arrow indicates flow direction. Final macrostructure is shown in Fig. 6(b).

the Bridgman furnace, at a pulling rate of 1 mm/s and a thermal gradient of 23 K/mm.[22] In the present work, it was shown that this type of dendrite mostly appears in the area of the highest thermal gradient, namely, the upstream edge of the cavity under conditions of forced flow. The development of curved arms is interrupted each time by the growth of the left-neighbor primary trunk followed by arm evolution on the neighbor dendrite. As a result, we observe the grain composed of many dendrites with a continuing line of curved secondary arms (Figure 11(b), left grain).

### B. *Grain Deflection*

As described in Section IV, the columnar dendrites are deflected toward the incoming flow; this has been reported by many researchers. In the present scheme of the experiment, it is rather difficult to determine the correlations between the grain deflection and the flow conditions, due to the strong vorticity. However, some qualitative relations were obtained in grain growth by comparing the deflection angle of the grains with the shape of the isotherms during solidification (Figures 6 and 10).

Additionally, it was shown that the dendrites may change the grain growth direction during progressing solidification (Figure 9(b)). High superheat decreases the solidification rate and increases the thermal gradient, promoting the increase in the $G/V$ ratio and the change in the structure morphology from dendritic columnar to undeveloped columnar, as discussed earlier (Figure 7). This fact disposes of the difficulty related to the competitive growth between the primary and secondary arms. Consequently, the resulting orientation of the columnar dendrites will depend on the direction of the thermal and solutal gradient.

On the other hand, at a constant velocity, the flow decreases the solidification rate in the vertical section with an associated change in microstructural features, *e.g.*, the increasing of the primary dendrite arm spacing. This facilitates an intensive branching with a high probability of orientation change.

Another reason for the change in the growth orientation is the inflow of the superheated melt, which promotes the detachment of the growing dendrite arms and, again, the change from the dendritic-columnar to the undeveloped-columnar structure. Another important factor affecting the growth orientation may be the transport of detached fragments. If the survival of fragments in the superheated melt becomes possible, they can be incorporated at the solidification front and, under certain conditions involving a high thermal gradient, can give rise to columnar grains of new orientation.

Some of the dendrites were deflected (Figure 6(a), zone 1), and the dendrite branches (Figure 9(a)) were growing in the downstream direction with respect to the forced flow. These observations can be most probably explained by the vortices clearly visible in the results of the computer simulations of the flow field. The vortices, which appear after the first seconds of the onset of solidification, alter the thermal field in the cavity; the dominating thermal gradients turn the growth of the dendrite and its branches in the downstream direction. As is shown in Section IV, the plastic deformation may occur during the solidification of an Al-4.5 pct Cu alloy and, consequently, may promote the deflection of the dendrites in the direction of flow. However, to find out what mechanism contributes more to the downstream deflection of dendrites was not possible within the scope of this study.

### C. *Dendrite Arm Spacing*

The increasing flow velocity is found to reduce the distance between the growing primary trunks. However, at a constant flow velocity, the intensive branching of high-order dendrite arms can be observed as the distance from the chill surface increases. This explanation conforms with the structure data in Figure 12, where the decreasing of the solidification and cooling rates corresponds to the increasing of the distance from the chill surface.

The solidification time is the dominant factor for the secondary dendrite arm spacing. More effective melt transport to the growing branches in the interdendritic region leads to their coarsening under forced-flow

conditions (Figure 13). The experimentally obtained values of the secondary dendrite arm spacing can be fitted to the power law[23]

$$\lambda_2 = K(Mt_s)^n \qquad [2]$$

where

$$M = -\frac{\Gamma D}{(1-k_o)m_L(C_E - C_0)} \ln\left(\frac{C_E}{C_0}\right) \qquad [3]$$

where $K = 5$ (according to Kirkwood[24]). For an Al-4.5 wt pct Cu alloy, $D$ is the solute diffusivity in the liquid phase ($3 \cdot 10^{-9}$ m$^2$ s$^{-1}$), $m_L$ is the slope of the liquidus line (–3.4 K pct Cu$^{-1}$), $k$ is the alloy partition coefficient (0.19), $C_0$ is the bulk solute concentration (4.5 pct Cu), $C_E$ is the eutectic solute concentration, and $\Gamma$ is the Gibbs–Thompson coefficient ($2.4 \cdot 10^{-9}$ m K). As can be seen, this expression can be fitted to the measured values with the coarsening constant $n$ as a fitting parameter. The coarsening parameter varies from 0.31 to 0.52, depending on the bulk-flow velocity for certain heat conditions (Figure 13). Evidently, the more pronounced coarsening is shown on the samples obtained at a higher superheat and at higher flow velocities. Diepers *et al.*[25] numerically studied the interaction between melt flow and ripening in a solidification microstructure, using a phase-field model. The main outcome of their work is the demonstration that the coarsening exponent changes from 1/3 for diffusion-controlled ripening to 1/2 under a convective regime, which corresponds well to the results given in Figure 13. Our results are also in agreement with a ripening theory proposed earlier by Ratke and Thieringer.[26] Recently, the experiments with well-defined and controlled conditions were performed by Steinbach and Ratke,[5] with the results agreeing.

## VI. CONCLUDING REMARKS

The chill with cavity has been applied to study the effect of forced flow on the unsteady-state solidification of an Al-4.5 pct Cu alloy. The present article provides a better understanding of the flow phenomena and their associated complex effects on solidification in a rectangular cavity under forced-flow conditions. The cavity-driven flow with solidification is determined by several interacting features. The high velocity gradient between the forced incoming flow and the flow inside the cavity results in the development of instabilities that tend to stretch in a longitudinal direction due to the dynamic change in the geometric ratio with progressing solidification. The macrovortices occurring at the earlier stage of solidification may represent scaled-up interaction between the solidification front and the flow pattern in any industrial casting process, including both natural and forced convection.

The results of this work can be summarized as follows. The flow lowers the solidification rate, while the thermal gradient does not change much. This results in an increasing $G/V$ ratio, and the corresponding morphology changes from dendritic columnar to undeveloped columnar.[18] The zone of equiaxed grains on the downstream side of the cavity under conditions of optimum heat inflow might partially consist of fragments formed as a result of a strong, forced flow. This hypothesis was supported by several arguments. The ECT, atypical for the conventional cast structure, is found to be a result of the termination of the fragmentation and the continuous deposition of detached branches, due to the change in cavity depth. The high temperature gradient maintained during experiment results in subsequent columnar growth. The peculiar morphology, such as feathery grains and curved dendrites, strongly depends on the solidification parameters determined by the forced flow. The growth direction of the dendrites is also dominated by the forced flow. The pronounced growth on the upstream side of the trunk may be associated with a vortex flow structure. One of the most interesting results is the correlation between microstructure, solidification, and flow parameters, which indicates an increase in the coarsening constant in the well-known power law, due to the flow velocity under conditions of identical thermal gradient and initial superheat.

## ACKNOWLEDGMENTS

This work is done within the framework of the research program of the Netherlands Institute for Metals Research (www.nimr.nl), Project MC 4.02134. The authors thank J.J.H. van Etten, J.J. Jansen, and J. Boomsma for practical assistance in preparing and performing the experiments.

## REFERENCES

1. K. Murakami, T. Fujiyama, A. Koike, and T. Okamoto: *Acta Mater.*, 1983, vol. 31, pp. 1425–32.
2. A. Buchholz and S. Engler: *Comput. Mater. Sci.*, 1996, vol. 7, pp. 221–27.
3. M. Guo, Y. Yang, F. Hua, and Z. Hu: *Z. Metallkd.*, 2004, vol. 95, pp. 835–39.
4. W.D. Griffits and D.G. McCartney: *Mater. Sci. Eng. A*, 1996, vol. 216, pp. 47–60.
5. S. Steinbach and L. Ratke: *Mater. Sci. Eng. A*, 2005, vols. 413–414, pp. 200–04.
6. R.S. Rerko, H.C. de Groh, III, and C. Beckermann: *Mater. Sci. Eng. A*, 2003, vol. 347, pp. 186–97.
7. P.A. Nikrityuk, K. Eckert, and R. Grundmann: *Int. J. Heat Mass Transf.*, 2006, vol. 49, pp. 1501–15.
8. P.A. Nikrityuk, K. Eckert, B. Willers, and S. Eckert: in *Modeling of Casting, Welding and Advanced Solidification Processes XI*, C.A. Gandin and M. Bellet, eds., TMS, Warrendale, PA, 2006, pp. 333–40.
9. A. Turchin, D.G. Eskin, and L. Katgerman: *Mater. Sci. Eng. A*, 2005, vols. 413–414, pp. 98–104.
10. C.M. Oldenburg and F.J. Spera: *Numer. Heat. Transf. B*, 1992, vol. 21, pp. 217–29.
11. M.R. Barkhudarov and C.W. Hirt: in *Modeling of Casting, Welding, and Advanced Solidification Processes VII*, M. Cross and J. Campbell, eds., TMS, Warrendale, PA, 1995, pp. 935–46.
12. H. Grazzini and D. Nesa: in *Solidification Processing '97*, University of Sheffield, Sheffield, United Kingdom, 1997, pp. 147–50.
13. J. Zuidema, Jr.: Doctoral Thesis, Delft University of Technology, Delft, The Netherlands, 2005, pp. 89–103.
14. C.J. Vreeman and F.P. Incropera: *Int. J. Heat Mass Transf.*, 2000, vol. 43, pp. 687–704.

15. H. Yao, R.K. Cooper, and S. Raghunathan: *J. Fluids Eng*., 2004, vol. 126, pp. 919–27.
16. R. Trivedi, H. Miyahara, P. Mazumder, E. Simsek, and S.N. Tewari: *J. Cryst. Growth*., 2001, vol. 222, pp. 365–79.
17. T. Okamoto, K. Kishitake, and I. Bessho: *J. Cryst. Growth*, 1975, vol. 29, pp. 131–36.
18. W. Kurz and D.J. Fisher: *Fundamentals of Solidification*, 3rd ed., Trans Tech Publications Ltd, Aedermannsdorf, Switzerland, 1992.
19. J. Pilling and A. Hellawell:: *Metall. Mater. Trans. A*, 1996, vol. 27A, pp. 229–32.
20. D.G. Eskin, Suyitno, and L. Katgerman: *Progr. Mater. Sci*., 2004, vol. 49, pp. 629–711.
21. A.N. Turchin, D.G. Eskin, and L. Katgerman: in *Continuous Casting*, H.R. Müller, ed., Wiley-VCH, Weinheim, Germany, 2005, pp. 283–89.
22. S. Henry, T. Minghetti, and M. Rappaz: *Acta Mater*., 1998, vol. 46, pp. 6431–43.
23. U. Feurer: in *Quality Control of Engineering Alloys and The Role of Metals Science*, H. Nieswaag and J.W. Schut, eds., Delft University of Technology, Delft, The Netherlands, 1978, pp. 131–45.
24. D.H. Kirkwood: *Mater. Sci. Eng*., 1985, vol. 73, pp. L1–L4.
25. H.J. Diepers, C. Beckermann, and I. Steinbach: *Acta Mater*., 1999, vol. 47, pp. 3663–78.
26. L. Ratke and W.K. Thieringer: *Acta Metall*., 1985, vol. 33, pp. 1793–1802.